

Performance Evaluation of Liquid Cooling Systems in 18650 Batteries: A Case Study of Mass Flow Rate Variations in Mini-Channel Cold Plates

Rainer Samuel Fourlando¹, James Julian^{1*}, Anggie Topan Wijaya¹, Fitri Wahyuni¹, Riki Hendra Purba¹, Fathin Muhammad Mahdhudhu², Elvi Armadani³

¹Departement of Mechanical Engineering, Universitas Pembangunan Nasional Veteran Jakarta

²Departement of Naval Architecture, Universitas Pembangunan Nasional Veteran Jakarta

³Departement of Industrial Engineering, Universitas Pembangunan Nasional Veteran Jakarta
Jl. Rs. Fatmawati, Pondok Labu, Kota Jakarta Selatan 12450, Indonesia

zames@upnvj.ac.id

Abstrak

Pengelolaan energi termal secara efektif sangat penting untuk kinerja optimal, keamanan, dan umur pakai baterai lithium-ion, yang menghasilkan panas yang signifikan selama operasi. Suhu yang berlebihan dapat menyebabkan penurunan kapasitas dan thermal runaway. Studi ini secara numerik menyelidiki kinerja termal sistem pendingin cair menggunakan pelat pendingin mini-channel untuk modul delapan baterai lithium-ion silinder. Tujuan utama adalah mengevaluasi dampak perubahan laju aliran massa pendingin terhadap suhu maksimum baterai dan keseragaman suhu. Model dinamika fluida komputasional (CFD) yang telah diverifikasi dengan data eksperimental digunakan untuk analisis. Tiga konfigurasi laju aliran massa yang berbeda disimulasikan. Hasil menunjukkan efisiensi tinggi sistem, dengan suhu maksimum baterai tetap di bawah 26,5°C pada semua konfigurasi. Ini mewakili pengurangan lebih dari 49% dibandingkan dengan skenario tanpa pendinginan, di mana suhu melebihi 52°C. Laju aliran massa tertinggi menghasilkan kinerja terbaik, mencapai pengurangan suhu 50,5% dan berhasil menjaga perbedaan suhu internal di bawah ambang kritis 5°C. Temuan ini menunjukkan bahwa sistem pendingin cair tidak hanya mencegah thermal runaway tetapi juga berkontribusi pada perpanjangan umur siklus baterai.

Kata kunci: Pelat Pendingin, Sistem Pendingin, Baterai Lithium-ion, Laju Aliran Massa, Suhu.

Abstract

Managing thermal energy effectively is essential for the optimal performance, safety, and lifespan of lithium-ion batteries, which generate substantial heat during operation. Excessive temperatures can lead to capacity degradation and thermal runaway. This study numerically investigates the thermal performance of a liquid cooling system using a mini-channel cold plate for a module of eight cylindrical lithium-ion batteries. The primary objective is to evaluate the impact of varying the coolant mass flow rate on the maximum battery temperature and temperature uniformity. A computational fluid dynamics (CFD) model, validated against experimental data, was employed for the analysis. Three distinct mass flow rate configurations were simulated. The results demonstrate the system's high efficiency, maintaining the maximum battery temperature below 26.5°C across all configurations. This represents a reduction of over 49% compared to the uncooled scenario, where temperatures exceeded 52°C. The highest mass flow rate yielded the best performance, achieving a temperature reduction of 50.5% and successfully keeping the internal temperature difference below the critical threshold of 5°C. These findings indicate that the liquid cooling system not only prevents thermal runaway but also contributes to prolonging battery cycle life.

Keywords: Cold plate, cooling system, lithium-ion batteries, mass flow rate, temperature.

NOMENCLATURE

		K	Thermal Conductivity
		\dot{m}	Mass Flow Rate
C_p	Specific Heat Capacity	Q_{GEN}	Volumetric Heat Generation Rate

T	Temperature (Celsius)
T_{MAX}	Maximum Temperature
T_{AVG}	Average Temperature
ΔT	Temperature Difference
u, v, w	Velocity Components in the x, y, z directions
z, y, z	Cartesian Coordinates
μ	Dynamic Viscosity
ρ	Density
r	Grid Refinement Ratio
\bar{p}	Convergence Order
f_1	Simulation Result with Fine Mesh
f_2	Simulation Result with Medium Mesh
f_3	Simulation Result with Coarse Mesh
GCI	Grid Convergence Index
F_s	Factor Of Safety
ϵ	Absolute Error
$f_{r=0}$	True Error

I. INTRODUCCION

As the demand for renewable energy sources increases, the issue of energy storage has become crucial in addressing the mismatch between supply and demand, as well as the instability inherent in these sources. [1]. The battery industry has seen rapid innovation driven by the need for new energy storage technologies, with batteries now emerging as a key solution [2]. The field of energy storage has seen significant expansion due to the superior characteristics of lithium-ion (Li-ion) batteries, including high energy density, long service life, and good charge retention. [3]. Nonetheless, a pivotal issue concerning lithium-ion batteries pertains to the generation of substantial quantities of heat while it is charging and discharging. This phenomenon exerts a direct influence on the performance and safety of the batteries, as elevated temperatures can precipitate thermal runaway and capacity degradation [4]. This is usually because the separator inside the battery can melt at high temperatures, resulting in direct contact with the electrodes and ultimately causing uncontrolled heating [5]. Consequently, it is very important to manage the battery's temperature is kept safely. The best temperature for the battery is between 25°C and 45°C [6]. In line with these needs, over the past five years, numerous studies have focused on battery cooling, particularly using liquid coolants and active systems [7], [8]. For Li-ion

batteries to operate safely and efficiently, two critical thermal thresholds must be respected. Firstly, the peak temperature of any single cell must be kept from exceeding 50°C to prevent thermal degradation. Secondly, to ensure balanced performance and longevity across the entire module, the temperature difference between individual cells must be maintained below 5°C [9].

Zhou et al. [10] demonstrated that novel liquid cooling configurations, specifically half-helical ducts, show great potential for single 18650 cells. However, the complexity of this design limits its applicability at the module level. To address thermal uniformity issues in larger battery packs, subsequent studies explored hybrid strategies, such as combining liquid cooling with air [11], utilizing thermoelectric coolers (TEC) [12], or integrating Phase Change Materials (PCM) [13]. While these hybrid approaches are effective, they frequently result in increased system weight, complexity, and parasitic power consumption. In terms of safety, Xiao et al. [14] highlighted the capability of liquid cooling to retard the spread of thermal runaway. Furthermore, Gao et al. [15] introduced a significant advancement with the Gradient Channel Design (GCD), which effectively minimizes temperature gradients by adapting channel geometry. Despite these technological strides, maintaining optimal $\Delta T < 5^\circ\text{C}$ in cylindrical battery modules without incurring major design trade-offs remains a critical challenge.

This research addresses the need for practical cooling systems by focusing on a mini-channel cold plate that uses water as the working fluid. In this design, heat is transferred radially from the battery cell to the cold plate. To evaluate the system's effectiveness in reducing temperature and maintaining battery durability, the performance will be analyzed at three distinct mass flow rates: 0.0005, 0.0015, and 0.0025 kg/s. These relatively low mass flow rates were selected to align with low C-rate battery operation.

II. RESEARCH METHODOLOGY

The research methodology, shown in Figure 1, comprises three stages: pre-processing, processing, and post-processing. The pre-processing stage begins with a literature study. The processing stage includes a verification and validation check. Finally, valid results enter the post-processing stage for data analysis and conclusion.

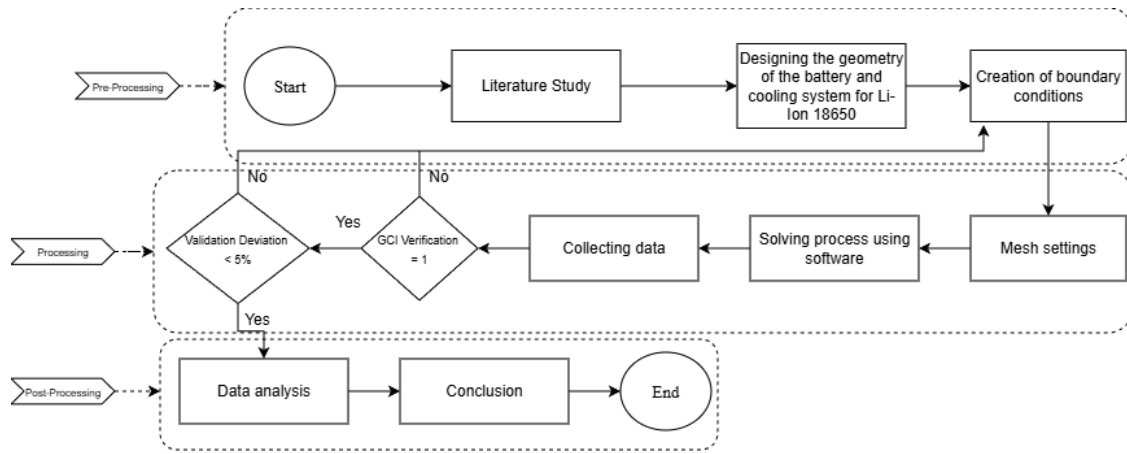


Figure 1. Research Procedure Flowchart

Lithium-Ion Battery Model

Research on this occasion focuses on the liquid cooling system applied to cylindrical batteries. The 18650 Lithium-ion cell type, with commercial specifications that enable discharge rates ranging from 15 to 30 Ampere. Figure 2 provides a visual representation of the battery's dimensions. This study considers the battery pack model arrangement to be homogeneous with respect to its thermal properties.

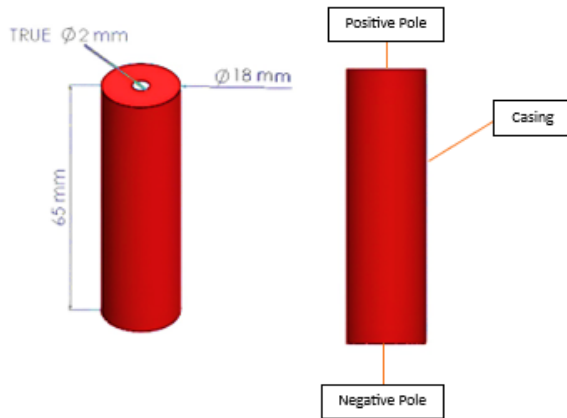


Figure 2. Specifications of Geometry and Spatial Dimensions for the 18650 Lithium-Ion

Cold Plate Architectures with Mini-Channels

Figure 3 depicts the layout of the eight-battery module analyzed in this research. There are two parallel rows with four cells each. This configuration was strategically chosen to distribute the thermal load generated during operation, and a direct liquid cooling strategy centered on mini-channel cooling plates was implemented. Aluminum is utilized for these components to ensure efficient heat conduction through direct contact with the base of the cells. The design framework also establishes essential configurations, such as the battery positioning, cold plate geometry, and inlet sizing. Aluminum was deliberately chosen for its combination of high

thermal conductivity, as shown in Table 1, which facilitates rapid heat transfer from the cells to the coolant.

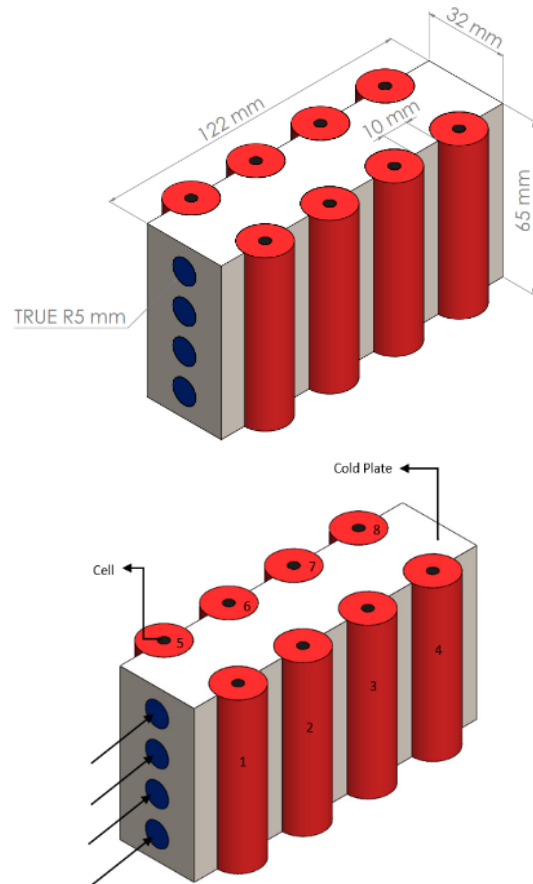


Figure 3. Visualization of The Configuration Mini-Channel Cold Plate Integrated Into The Battery Pack

Governing Equations

This investigation made use of the RANS method to achieve a precise simulation of fluid dynamics, particularly in the mini-channel, due to the circulation of coolant fluid. The equations solved refer to (1), Mass Conservation (Continuity Equation), thereby ensuring the preservation of fluid mass throughout the domain.

Table 1. The Material Properties Conditions

Material	ρ (kg.m ⁻³)	C_p (J.kg ⁻¹ .k ⁻¹)	k (W.m ⁻¹ .k ⁻¹)	μ (Pa.s)
Aluminum	2179	871	202.4	-
Battery Cell	2534.26	1558.3	3.02	-
Water	998.2	4128	0.6	1.03×10^{-3}

The fluid motion, including its pressure and viscous forces, is modeled with reference to (2). The heat equation in solids for thermal dissipation, such as in battery cells, is given in three dimensions with reference to (3). For the solid domain, the heat generation rate is defined by (4). Furthermore, to capture more complex thermal scenarios, (5) is utilized to account for both inhomogeneous (non-uniform) and transient heat transfer phenomena.

$$\frac{\partial \rho}{\partial t} + \frac{\partial}{\partial x_i}(\rho u_i) = 0 \quad (1)$$

$$\begin{aligned} \frac{\partial}{\partial t}(\rho u_i) + \frac{\partial}{\partial x_i}(\rho u_i u_j) &= \frac{\partial p}{\partial x_i} \\ + \frac{\partial}{\partial x_j} \left[\mu \left(\frac{\partial u_i}{\partial x_j} + \frac{\partial u_j}{\partial x_i} - \frac{2}{3} \delta_{ij} \frac{\partial u_k}{\partial x_k} \right) \right] & \quad (2) \\ + \frac{\partial}{\partial x_i}(-\rho \overline{u_i' u_j'}) & \end{aligned}$$

$$\rho C_p \frac{\partial T}{\partial t} = \lambda_x \frac{\partial^2 T}{\partial x^2} + \lambda_y \frac{\partial^2 T}{\partial y^2} + \lambda_z \frac{\partial^2 T}{\partial z^2} + Q_{gen} \quad (3)$$

$$Q_{gen}(t) = \rho C_p \frac{\Delta T}{\Delta t} \quad (4)$$

$$Q_{gen(1-2)}(x,y,z,t) = Q_{gen(1-2)}(t) - \lambda \nabla^2 T_{(1-2)} \quad (5)$$

Meshing and Boundary Conditions

The computational domain, which includes the cylindrical 18650 battery cells and the mini-channel cold plate, was discretized with an unstructured mesh. A mesh made up of tetrahedral elements was used for both the solid and fluid domains. Specifically, this method is flexible enough to accurately capture the complex geometric interface. Figure 4 shows the final mesh for the whole part.



Figure 4. Unstructured Mesh Configuration

Table 2 outlines the various mass flow rates applied within the cooling model, where a constant channel diameter of 10 mm was maintained across all simulation scenarios. The mass flow rate has been designated as the primary independent variable because it exerts a direct influence on the system's overall heat removal capacity and the convective heat transfer coefficient. As shown in Figure 5, which is visualized in cross-section, the working fluid (water) flowing inside the four channel plates is assumed to move from the inlet toward the outlet.

Table 2. Parameter Variations in This Study

Diameter Inlet (mm)	Mass Flow Rate (kg/s)
10	0.0005
	0.0015
	0.0025

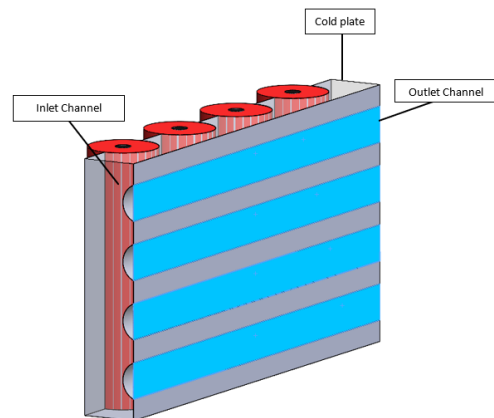


Figure 5. Boundary Conditions of The Mini-Channel Cold Plate in Liquid Cooling Systems

Mesh Independence Test

To quantify the discretisation error, a mesh sensitivity study was conducted. The methodology is based on the Grid Convergence Index introduced by Roache [16]. The number of elements in each mesh is constrained by a grid refinement ratio, as defined in (6). The observed order of convergence, p , was then evaluated using (7). The error for each mesh level, fine and coarse, was calculated using the GCI formulas presented in (8) and (9). To ensure the validity of this error value, a condition that is verified using the test outlined in (11). Then, Equation (12) evaluates the results of this test to confirm the final error value.

Table 3 gives a summary of the results of the mesh independence test. After evaluating a coarse mesh of 878,804 elements and a medium mesh of 1,756,609 elements, the analysis indicated a GCI value below 5%, suggesting that the discretisation is within an acceptable range. The fine mesh was selected as the ideal configuration for this study. Therefore, a total of 3,511,218 fine grid elements were used for all subsequent simulations.

$$r = \frac{h_2}{h_1} \tag{6}$$

$$\bar{p} = \frac{\ln\left(\frac{f_3 - f_2}{f_2 - f_1}\right)}{\ln(r)} \tag{7}$$

$$GCI_{fine} = \frac{F_s |\epsilon|}{(r^{\bar{p}} - 1)} \tag{8}$$

$$GCI_{coarse} = \frac{F_s |\epsilon| r^{\bar{p}}}{(r^{\bar{p}} - 1)} \tag{9}$$

$$\epsilon = \frac{f_{n+1} - f_n}{f_n} \tag{10}$$

$$\frac{GCI_{fine}}{GCI_{coarse}} \approx 1 \tag{11}$$

$$f_{h=0} = f_1 + \frac{(f_1 - f_2)}{(r^{\bar{p}} - 1)} \tag{12}$$

Table 3. Mesh Independence Test Results

Criteria	Value		
\bar{p}	0.125530882		
r	2		
GCI_{fine}	0.043%		
GCI_{coarse}	0.0473%		
$\frac{GCI_{fine}}{GCI_{coarse}}$	1		
$Fr_h = 0$	34.8803		
Mesh Category	Fine	Medium	Coarse
Temp. Difference (°C)	34.8924	34.8935	34.8947
Error	0.03469%	0.03784%	0.04128%

III. RESULT AND DISCUSSION

Data Validation

An analysis of the data validation step confirms that the model accurately captures the underlying physical phenomena before being utilized for subsequent parametric studies. This analysis entails the comparison of experimental temperature data from prior studies. Nan Wang et al. [17] conducted experiments on 18650 cylindrical lithium-ion batteries, measuring the temperatures at the core and surface of the battery. The rate of discharge of the batteries was 2C in a test environment that was 35°C. These specific operating conditions are particularly relevant as the 2C discharge rate induces significant internal heat generation.

As illustrated in Figure 6, a high degree of consistency is observed between the numerical predictions and the experimental measurements. Maximum error margins of 3.914% (core) and 3.474% (surface) confirmed the reliability of the findings when compared to the reference data. These low error percentages indicate a high degree of quantitative agreement between the simulated and experimental outcomes.

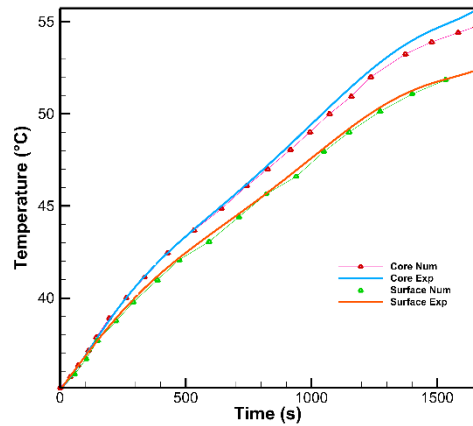
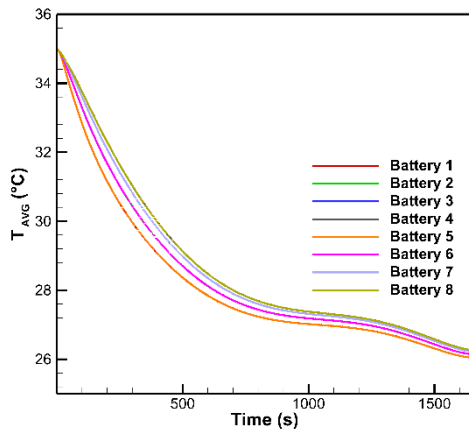


Figure 6. Comparison of Numerical Data with Experimental Data

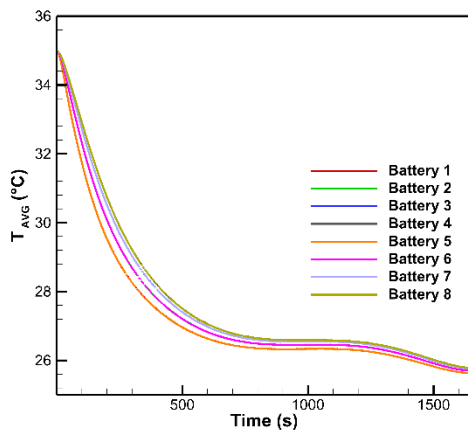
Analysis

Following the numerical model's verification, the study proceeds to analyze the thermal performance of the proposed liquid cooling system under various operational conditions. Figure 7 presents the transient response of the averaged temperature (T_{AVG}) for each of the eight battery cells. For this analysis, T_{AVG} is calculated as the arithmetic average of the max and min temperatures within each battery cell. The investigation was conducted for three distinct m: 0.0005 kg/s, 0.0015 kg/s, and 0.0025 kg/s while

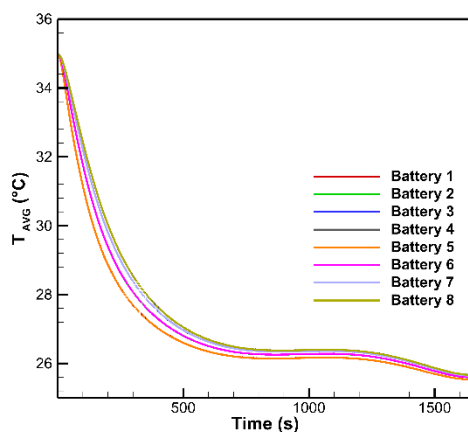
maintaining a constant channel diameter of 10 mm and a uniform initial battery temperature of 35°C.



(a)



(b)



(c)

Figure 7. Average Temperature Graph for Each of The Testing Variations \dot{m} (Kg/S) (A) 0.0005, (B) 0.0015, (C) 0.0025

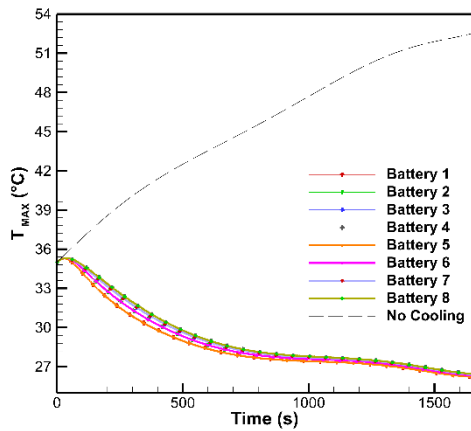
The results clearly demonstrate a significant and rapid thermal response from the cooling system. For all tested mass flow rates, the average temperature of every cell exhibits a pronounced decrease from the initial 35°C, eventually approaching a thermally stable condition near 25°C. This behavior is directly attributable to the principles of forced convection; a lower flow of liquid means the liquid moves more slowly through the small channels. This then makes the heat transfer coefficient go below a certain level. Consequently, the rate at which heat is extracted from the cold plate is less aggressive. Conversely, at higher mass flow rates, the enhanced fluid velocity promotes more effective heat transfer, leading to a more rapid temperature decline. Further analysis of the T_{AVG} graphs reveals a more gradual flattening. This indicates a slower rate of heat dissipation, meaning that the battery module takes a little longer to reach uniform temperature stability compared to the largest \dot{m} (0.0025 kg/s) in this study.

To illustrate the relationship between T_{MAX} in each battery across all mass flow rate variations over time, Figure 8 is presented. It is clear from the graph that there is a very significant decrease in battery T_{MAX} , where the graph shows a decline from the start of discharge. Starting with an initial temperature of 35°C and a time of 600 seconds, the temperature in the system did not increase. Instead, it decreased to a value close to 25°C in all configuration variations.

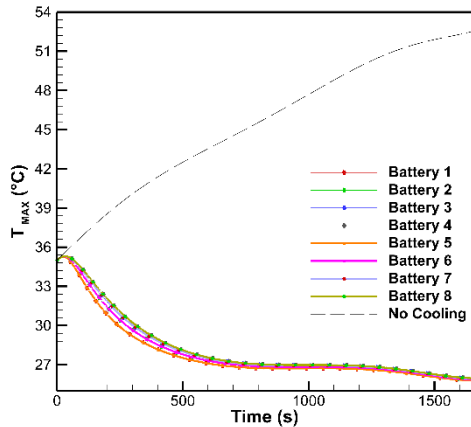
Comparing the T_{MAX} data (black dotted line) for the battery with the results from using a mini-channel cold plate reveals a significant difference. This shows that without this type of cooling system, the temperature will rise uncontrollably to almost 54°C, which is too hot for the battery to be safe to use. On the other hand, the T_{MAX} from all the simulations carried out during this study shows that the battery's maximum temperature continues to remain at an optimal performance level of about 25°C. This T_{MAX} value shows that the battery is working properly and is less likely to undergo thermal degradation due to heat.

The observed thermal phenomena can be elucidated in their fundamental essence by the precepts of heat transfer, which establish a correlation between heat absorbed by a moving fluid, its mass flow rate, and its temperature change. For a given and relatively constant heat generation rate from the battery module, according to this principle, the coolant's mass flow rate and its own temperature rise as it moves through the system are inversely related. At 0.0025 kg/s, the maximum mass flow rate, the fluid moves so rapidly that its temperature

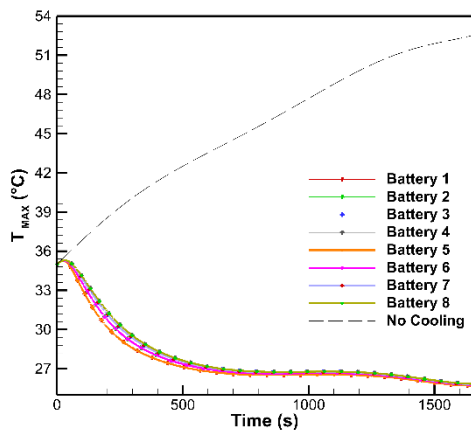
rise is minimal. This fundamental relationship, therefore, directly explains why increasing the mass flow rate is a highly effective strategy for improving thermal management performance.



(a)



(b)



(c)

Figure. 8. T_{MAX} Curve Under All Conditions \dot{m} (Kg/S) (A) 0.0005, (B) 0.0015, (C) 0.0025

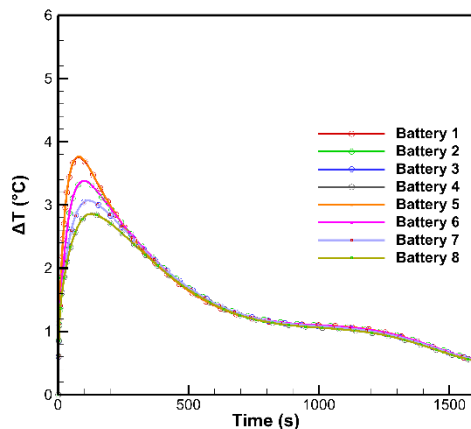
The effect of mass flow rate is more clearly seen in terms of response from the perspective of temperature difference (ΔT), as shown in Figure 9. The graph shows that $\dot{m} = 0.0005$ kg/s has the smallest trend in terms of ΔT , with the highest value still below 4°C , followed by $\dot{m} = 0.0015$ kg/s, which begins to show an increase in ΔT values but remains below 4°C for all batteries connected to the liquid cooling system using this model liquid cooling.

The relationship between mass flow rate and internal battery temperature difference (ΔT) is determined by the interaction between two different heat transfer mechanisms, internal conduction and external convection. In this context, ΔT represents the thermal gradient within a single cell, specifically the difference between the hotter core and the cooler surface ($T_{\text{CORE}} - T_{\text{SURFACE}}$). At low mass flow rates, such as 0.0005 kg/s, external convective cooling is weak and becomes the primary thermal resistance. Because heat removal from the battery surface is slow, the surface temperature remains high and approaches the core temperature.

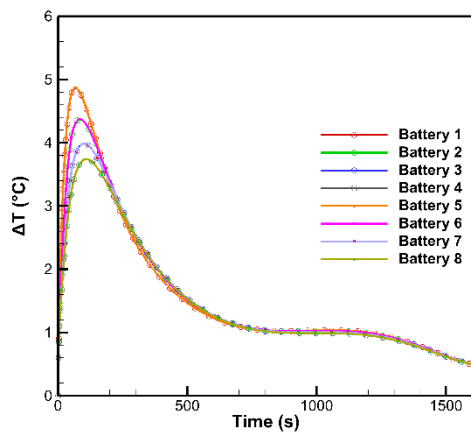
The analysis of the internal ΔT within each cell directly addresses the primary challenge outlined in the introduction. The overall explanation of ΔT throughout this battery is a response to the challenge outlined in the introduction, which states that achieving temperature uniformity below the critical limit of 5°C is necessary to prevent inconsistent degradation between cells. In this regard, all configurations demonstrate excellent ability to maintain uniform internal temperatures in each cell, and the results are very satisfactory even in the initial 500 seconds of the simulation. It is particularly noteworthy that even under the most aggressive cooling condition ($\dot{m} = 0.0025$ kg/s), where the peak ΔT is highest, the value only briefly exceeds the 5°C limit before rapidly declining. This indicates a robust and effective transient thermal response, before all ΔT values eventually stabilize below 2°C until the end of discharge. Ultimately, this demonstrates that the mini-channel cold plate design is highly capable of mitigating severe internal temperature gradients.

Table 4 presents a quantitative assessment of the thermal performance for each mass flow rate configuration. In the absence of cooling, the T_{MAX} escalates to 52°C , a level that would significantly accelerate cell degradation. In contrast, all three mass flow rate configurations successfully maintain the T_{MAX} below 26.5°C . This table shows an average reduction in peak temperature of 49.3% for the lowest flow rate and up to 50.5% for the highest flow rate. Furthermore, all configurations demonstrate an excellent ability to maintain uniform internal temperatures within each cell, with the internal temperature difference (ΔT) for every battery

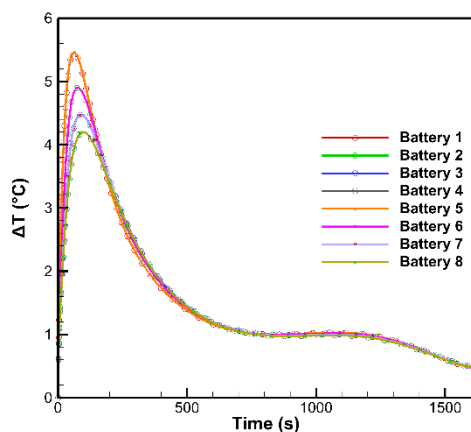
remaining below a very satisfactory 0.6°C at the end of the simulation.



(a)



(b)



(c)

Figure 9. Contrast of The Evolution of The Temperature Difference With Various \dot{m} (Kg/S) (A) 0.0005, (B) 0.0015, (C) 0.0025

This thermal improvement is further quantified in Table 5, which presents the effectiveness of each

configuration in terms of percentage temperature reduction relative to the uncontrolled, no-cooling scenario. At a flow rate of 0.0005 kg/s , the performance achieved an average temperature reduction of 49.3%. This demonstrates a substantial improvement over an unmanaged system. The configuration that works better than all the rest has a mass flow rate of 0.0025 kg/s , resulting in the highest average temperature reduction of 50.5%, with temperature reductions in individual cells reaching up to 50.6%. These results quantitatively prove that a bigger mass flow rate is superior in maximizing heat removal and achieving the lowest possible operational temperatures.

Beyond lowering the peak temperature, a higher mass flow rate also significantly improves the temperature uniformity across the entire module. This aspect is critical for ensuring balanced cell aging and maximizing the service life of the whole battery pack. In Figure 10, the temperature contours are clearly displayed visually. At $\dot{m} = 0.0005 \text{ kg/s}$, a pronounced temperature gradient is visible along the flow path, with the cold plate transitioning from the inlet to near the outlet. This visual evidence directly corresponds with the quantitative data in Table 4, where the temperature difference between the warmest and coolest cell is at its highest for this case. In contrast, at $\dot{m} = 0.0025 \text{ kg/s}$, the entire cold plate and battery assembly maintain a much more uniform temperature, indicating minimal temperature variation.

The underlying cause for this enhanced uniformity is revealed in the slice contour plots, which illustrate the thermal state of the working fluid within the mini-channels. For the 0.0005 kg/s case, the fluid itself shows a significant temperature increase, transitioning from the inlet to the outlet. This visualization confirms that the coolant becomes significantly warmer, thereby reducing its capacity to effectively cool the downstream batteries. This minimal temperature rise in the coolant signifies that its heat-carrying capacity is far from saturated, allowing it to provide a potent and consistent cooling effect to every cell it passes. In addition, possible future research could consider broader system implications, such as integrating liquid cooling strategies with hybrid or passive thermal management techniques. Expanding the investigation in this way will not only ensure a more holistic evaluation of thermal management solutions but also provide a stronger foundation for applying these findings to electric vehicles, aerospace systems, and stationary energy storage technologies, where efficiency, reliability, and cost-effectiveness must be carefully balanced.

Table 4. Quantitative Data of T_{MAX} and ΔT for Each Variation in Mass Flow Rate

	No Cooling System		$\dot{m} = 0.0005 \text{ kg/s}$		$\dot{m} = 0.0015 \text{ kg/s}$		$\dot{m} = 0.0025 \text{ kg/s}$	
Battery Cell	T _{MAX}	ΔT	T _{MAX}	ΔT	T _{MAX}	ΔT	T _{MAX}	ΔT
1	52 °C	0.0119 °C	26.23 °C	0.529 °C	25.80 °C	0.475 °C	25.70 °C	0.460 °C
2			26.33 °C	0.538 °C	25.87 °C	0.482 °C	25.76 °C	0.466 °C
3			26.41 °C	0.538 °C	25.93 °C	0.484 °C	25.81 °C	0.468 °C
4			26.45 °C	0.528 °C	25.96 °C	0.479 °C	25.83 °C	0.463 °C
5			26.23 °C	0.530 °C	25.80 °C	0.476 °C	25.70 °C	0.460 °C
6			26.33 °C	0.539 °C	25.88 °C	0.483 °C	25.76 °C	0.466 °C
7			26.41 °C	0.538 °C	25.93 °C	0.483 °C	25.81 °C	0.466 °C
8			26.45 °C	0.528 °C	25.96 °C	0.478 °C	25.83 °C	0.463 °C

Table 5. Cooling Effectiveness is Quantified by The Percentage Reduction in Maximum Temperature

	No Cooling System	$\dot{m} = 0.0005 \text{ kg/s}$	$\dot{m} = 0.0015 \text{ kg/s}$	$\dot{m} = 0.0025 \text{ kg/s}$
Battery Cell	T _{MAX}	Temp. Reduction (%)	Temp. Reduction (%)	Temp. Reduction (%)
1	52 °C	49.6%	50.4%	50.6%
2		49.4%	50.2%	50.4%
3		49.2%	50.1%	50.4%
4		49.1%	50.1%	50.3%
5		49.6%	50.4%	50.6%
6		49.4%	50.2%	50.4%
7		49.2%	50.1%	50.4%
8		49.1%	50.1%	50.3%
Average		49.3%	50.2%	50.5%

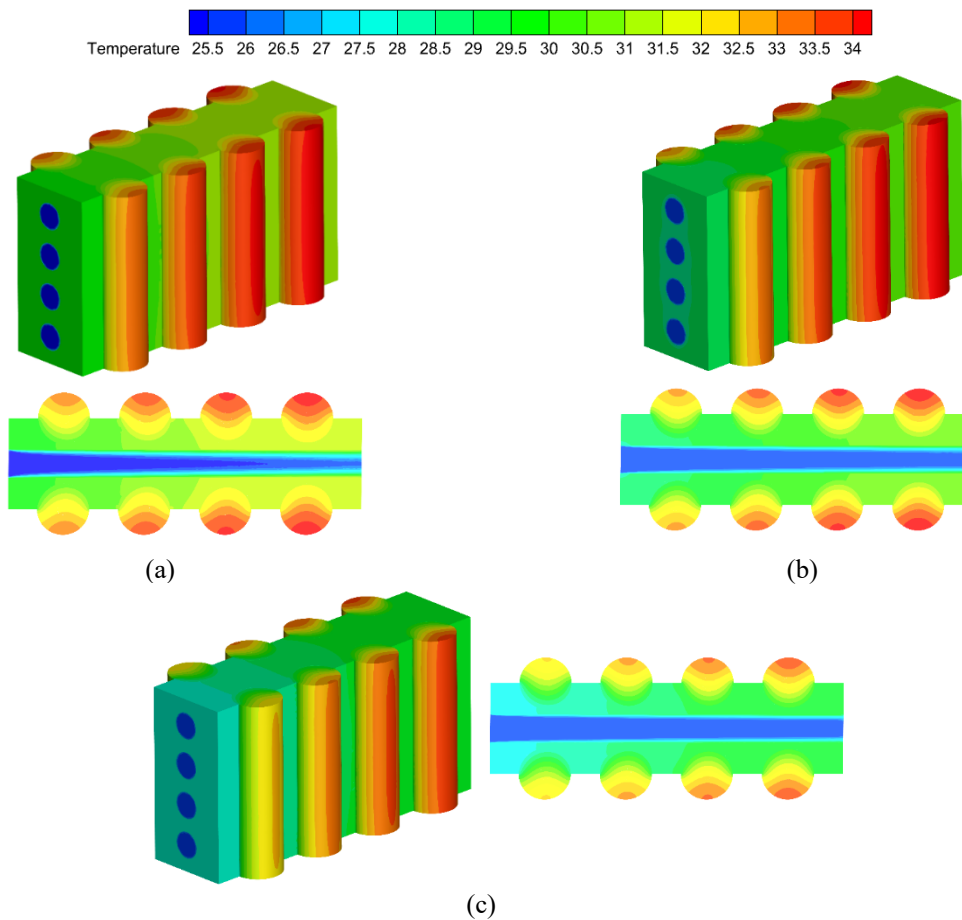


Figure 10. Temperature contours of each variation mass flow rate (a) 0.0005 kg/s, (b) 0.0015 kg/s, and (c) 0.0025 kg/s

IV. CONCLUSION

The system maintained the T_{MAX} below 26.5 °C across all tested configurations, representing an average temperature reduction of over 49% compared to the uncooled scenario. A clear positive correlation was found between the coolant mass flow rate and cooling performance. Raising the flow rate consistently lowered the maximum temperature and improved temperature homogeneity. The highest mass flow rate of 0.0025 kg/s exhibited the best performance, achieving the lowest T_{MAX} of 25.83 °C, the greatest temperature reduction of 50.5%, and a superior module-wide temperature difference of only 0.13 °C. Crucially, all configurations successfully maintained the ΔT within each cell below the critical 5 °C.

REFERENCES

- [1] X. R. R. Al-Fatlawy *et al.*, “Impact of Energy Storage Technologies on Grid-Connected Renewable Energy Systems,” *E3S Web Conf.*, vol. 591, p. 05006, 2024, doi: 10.1051/e3sconf/202459105006.
- [2] C. A. Rufino Júnior *et al.*, “Towards a business model for second-life batteries: Barriers, opportunities, uncertainties, and technologies,” *J. Energy Chem.*, vol. 78, pp. 507–525, Mar. 2023, doi: 10.1016/j.jechem.2022.12.019.
- [3] T. Chen *et al.*, “Applications of Lithium-Ion Batteries in Grid-Scale Energy Storage Systems,” *Trans. Tianjin Univ.*, vol. 26, no. 3, pp. 208–217, June 2020, doi: 10.1007/s12209-020-00236-w.
- [4] Z. Lei, Z. Maotao, X. Xiaoming, and G. Junkui, “Thermal runaway characteristics on NCM lithium-ion batteries triggered by local heating under different heat dissipation conditions,” *Appl. Therm. Eng.*, vol. 159, p. 113847, Aug. 2019, doi: 10.1016/j.applthermaleng.2019.113847.
- [5] Q. Wang, X. Zhao, J. Ye, Q. Sun, P. Ping, and J. Sun, “Thermal response of lithium-ion battery during charging and discharging under adiabatic conditions,” *J. Therm. Anal. Calorim.*, vol. 124, no. 1, pp. 417–428, Apr. 2016, doi: 10.1007/s10973-015-5100-4.
- [6] P. G. Zadeh, Y. Wang, and J. D. Chung, “Thermal management modeling for cylindrical lithium-ion battery packs considering safety and lifespan,” *J. Mech. Sci. Technol.*, vol. 36, no. 7, pp. 3727–3733, July 2022, doi: 10.1007/s12206-022-0646-0.
- [7] R. Zhou, Y. Chen, J. Zhang, and P. Guo, “Research progress in liquid cooling technologies to enhance the thermal management of LIBs,” *Mater. Adv.*, vol. 4, no. 18, pp. 4011–4040, 2023, doi: 10.1039/D3MA00299C.
- [8] Y. Deng *et al.*, “Effects of different coolants and cooling strategies on the cooling performance of the power lithium ion battery system: A review,” *Appl. Therm. Eng.*, vol. 142, pp. 10–29, Sept. 2018, doi: 10.1016/j.applthermaleng.2018.06.043.
- [9] Y. Lv, X. Yang, X. Li, G. Zhang, Z. Wang, and C. Yang, “Experimental study on a novel battery thermal management technology based on low density polyethylene-enhanced composite phase change materials coupled with low fins,” *Appl. Energy*, vol. 178, pp. 376–382, Sept. 2016, doi: 10.1016/j.apenergy.2016.06.058.
- [10] H. Zhou, F. Zhou, Q. Zhang, Q. Wang, and Z. Song, “Thermal management of cylindrical lithium-ion battery based on a liquid cooling method with half-helical duct,” *Appl. Therm. Eng.*, vol. 162, p. 114257, Nov. 2019, doi: 10.1016/j.applthermaleng.2019.114257.
- [11] H. Xiao, J. E. S. Tian, Y. Huang, and X. Song, “Effect of composite cooling strategy including phase change material and liquid cooling on the thermal safety performance of a lithium-ion battery pack under thermal runaway propagation,” *Energy*, vol. 295, p. 131093, May 2024, doi: 10.1016/j.energy.2024.131093.
- [12] Y. Lyu, A. R. M. Siddique, S. A. Gadsden, and S. Mahmud, “Experimental investigation of thermoelectric cooling for a new battery pack design in a copper holder,” *Results Eng.*, vol. 10, p. 100214, June 2021, doi: 10.1016/j.rineng.2021.100214.

- [13] W. Yang, F. Zhou, Y. Liu, S. Xu, and X. Chen, "Thermal performance of honeycomb-like battery thermal management system with bionic liquid mini-channel and phase change materials for cylindrical lithium-ion battery," *Appl. Therm. Eng.*, vol. 188, p. 116649, Apr. 2021, doi: 10.1016/j.applthermaleng.2021.116649.
- [14] W. Yang, F. Zhou, H. Zhou, Q. Wang, and J. Kong, "Thermal performance of cylindrical lithium-ion battery thermal management system integrated with mini-channel liquid cooling and air cooling," *Appl. Therm. Eng.*, vol. 175, p. 115331, July 2020, doi: 10.1016/j.applthermaleng.2020.115331.
- [15] R. Gao, Z. Fan, and S. Liu, "A gradient channel-based novel design of liquid-cooled battery thermal management system for thermal uniformity improvement," *J. Energy Storage*, vol. 48, p. 104014, Apr. 2022, doi: 10.1016/j.est.2022.104014.
- [16] P. J. Roache, "Perspective: A Method for Uniform Reporting of Grid Refinement Studies," *J. Fluids Eng.*, vol. 116, no. 3, pp. 405–413, Sept. 1994, doi: 10.1115/1.2910291.
- [17] N. Wang, A. Chen, W. Zhao, R. Zhu, and B. Duan, "An online temperature estimation for cylindrical lithium-ion batteries based on simplified distribution electrical-thermal model," *J. Energy Storage*, vol. 55, p. 105326, Nov. 2022, doi: 10.1016/j.est.2022.105326.

